ENGINEERING Agriculture

Engineering Journals

RESEARCH ARTICLE

2027 / Volume 14 / Issue 2 / 27724

Parameter calibration method for discrete element simulation of cut seed potato tubers

Niu QI[1,2,3], Rongxiang DIAO[1], Rui RAN[1], Hongnan HU[4], Zhongcai WEI[5], Mingsheng LI[1,2,3], Chengsong LI[1,2,3], Pei WANG (✉)[1,2,3]

1 College of Engineering and Technology, Southwest University, Chongqing 400715, China.
2 Chongqing Key Laboratory of Intelligent Agricultural Equipment in Hilly and Mountainous Areas, Chongqing 400715, China.
3 Southwest Mountain Regions Intelligent Agricultural Machinery Equipment Innovation Center, Southwest University, Chongqing 400715, China.
4 College of Mechanical and Electrical Engineering, Zhongkai University of Agriculture and Engineering, Guangzhou 510225, China.
5 School of Agricultural Engineering and Food Science, Shandong University of Technology, Zibo 255091, China.

KEYWORDS

Angle-of-repose optimization, cut seed potato tuber, discrete element method, electromagnetic vibration seed-feeding device

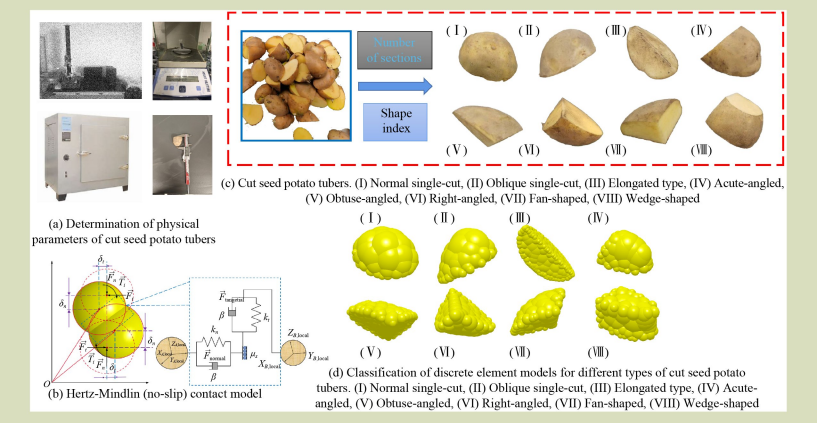
HIGHLIGHTS

- A classified discrete element method (DEM) modeling method based on cut surface count was developed to accurately represent seed potato shape variability.
- Contact parameters were calibrated via integrated physical tests and DEM optimization.
- Inter-tuber friction parameters were identified using Plackett-Burman, steepest ascent and Box-Behnken response surface methodology.
- The calibrated model predicted angle of repose with a relative error of 1.27%.
- DEM simulations agreed well with electromagnetic vibrating feeder tests, showing errors below 5% in discharge time and mass flow rate.

Received January 22, 2025;
Accepted May 7, 2026.

Correspondence: peiwang@swu.edu.cn

GRAPHICAL ABSTRACT



ABSTRACT

The shape of materials significantly affects their kinematic properties. In discrete element method (DEM) simulations, accurately modeling both the shape and mechanical properties of materials is essential. Thus, this paper proposes a modeling approach based on the number of cut surfaces on cut seed potato tubers. To develop accurate models, the intrinsic parameters of cut seed potato tubers with varying numbers of cut surfaces were measured. Drop tests, pendulum tests and inclined-plane tests were used to calibrate the coefficients of restitution, static friction and rolling friction for tuber-steel plate interactions, as well as the inter-tuber coefficient of restitution. A comprehensive approach combining Plackett-Burman design, the method of steepest ascent and Box-Behnken response surface methodology was used to calibrate the inter-tuber friction parameters, yielding static and rolling friction coefficients of 0.453 and 0.024, respectively. Validation with the pumping

plate method showed a relative error of 1.27% between the simulated and measured angles of repose. In feeding tests using an electromagnetic vibrating hopper, the simulation results differed from the experimental results by less than 5%. These calibrated parameters provide a robust theoretical basis for designing and analyzing cut seed potato planting equipment.

© The Author(s) 2027. Published by Higher Education Press. This is an open access article under the CC BY license (http://creativecommons.org/licenses/by/4.0)

1 Introduction

Potato (*Solanum tuberosum*) is one of the global major crops and plays a crucial role in sustainable agricultural development[1,2]. China produced 27.1% of global potato production in 2023[3], making it one of the major potato-producing countries, with a cultivation area of about 4.6 Mha[4]. Ninety percent of potatoes are sown using cut seed tubers in China. The cut seed tubers are classified into single, double- and triple-cut-surfaces types based on the number of cut surfaces[5]. These cut tubers have significantly different dynamic characteristics owing to their different cut surface configurations. Since the motion of cut seed potato tubers within the sowing machine is inherently complex and cannot be accurately predicted solely by theoretical calculations, considerable challenges are presented in the optimization of cut seed potato sowing equipment.

The discrete element method can be applied in solving the issue mentioned above, as it has been widely used to analyze the motion of many agricultural materials[6–10]. Studies by Liu et al.[11], Shi et al.[12] and Chen et al.[13] demonstrated the feasibility of establishing DEM models for potatoes, especially for the mini-tubers in ellipsoidal or spherical shapes. Substantial studies had addressed the calibration of DEM parameters for other materials. For seeds with regular shapes, such as soybeans[14], simplified spherical or ellipsoidal models were commonly adopted. For seeds with irregular shapes, such as sunflower seeds[15], equivalent-volume spherical particles[16] combined with multi-sphere[17] or polyhedron methods[18] are typically used to represent non-spherical particle shapes.

The main calibration parameters required for DEM simulations include intrinsic parameters and contact parameters[19]. Intrinsic parameters can be determined through direct measurements, such as compression tests for elastic modulus[20] and water-displacement methods for density[21]. However, due to discrepancies in geometry and contact characteristics between simulated particles and real materials, contact parameters must be calibrated through a combination of physical tests and simulation-based calibration[22]. Physical tests commonly include high-speed imaging for the coefficient of restitution[23], inclined-plane sliding tests for the static friction coefficient[24,25] and rotating drum tests for the rolling friction coefficient[26]. For agricultural materials with pronounced shape variability, the material-material friction coefficients are often difficult to measure directly. Consequently, statistical optimization is widely used for simulation-based calibration, including the Plackett-Burman design, the method of steepest ascent and response surface methodology[27–29], as well as genetic algorithms[30], to identify key factors and obtain reliable DEM parameters.

Thus, to support the optimization of potato sowing machines in China, it is essential to establish accurate DEM models of cut seed potato tubers. The objectives of this study were: (1) to measure the intrinsic parameters of cut seed potato tubers and develop DEM models based on different numbers of cut surfaces and morphological characteristics; (2) to calibrate the coefficient of restitution and friction parameters for the optimization of inter-tuber interaction parameters; and (3) to validate the calibrated parameters through pumping plate method and electromagnetic vibrating feeder tests.

2 Materials and methods

2.1 Determination of intrinsic parameters of cut seed potato tuber and establishment of discrete element model

The potato cultivar Dutch No. 15, widely cultivated in China, was used in this study. To determine the triaxial dimensions and shape indices of cut seed potato tubers, the cutting methods specified in NY/T 3483-2019[31] and the statistical

proportions of different cut-surface types were used as references. One hundred samples were randomly selected, including 13 single-cut-surface tubers, 31 double-cut-surface tubers and 56 triple-cut-surface tubers (Table1). During measurement, the tubers were first classified according to the number of cut surfaces. Subsequently, a vernier caliper with an accuracy of 0.02 mm (Fig. 1(a)) was used to measure the three orthogonal dimensions of each cut seed potato tuber, and the corresponding shape index was calculated as:

$$f_s = \frac{a_{\max}^2}{b_{\max} \times c_{\max}} \times 100\% \quad (1)$$

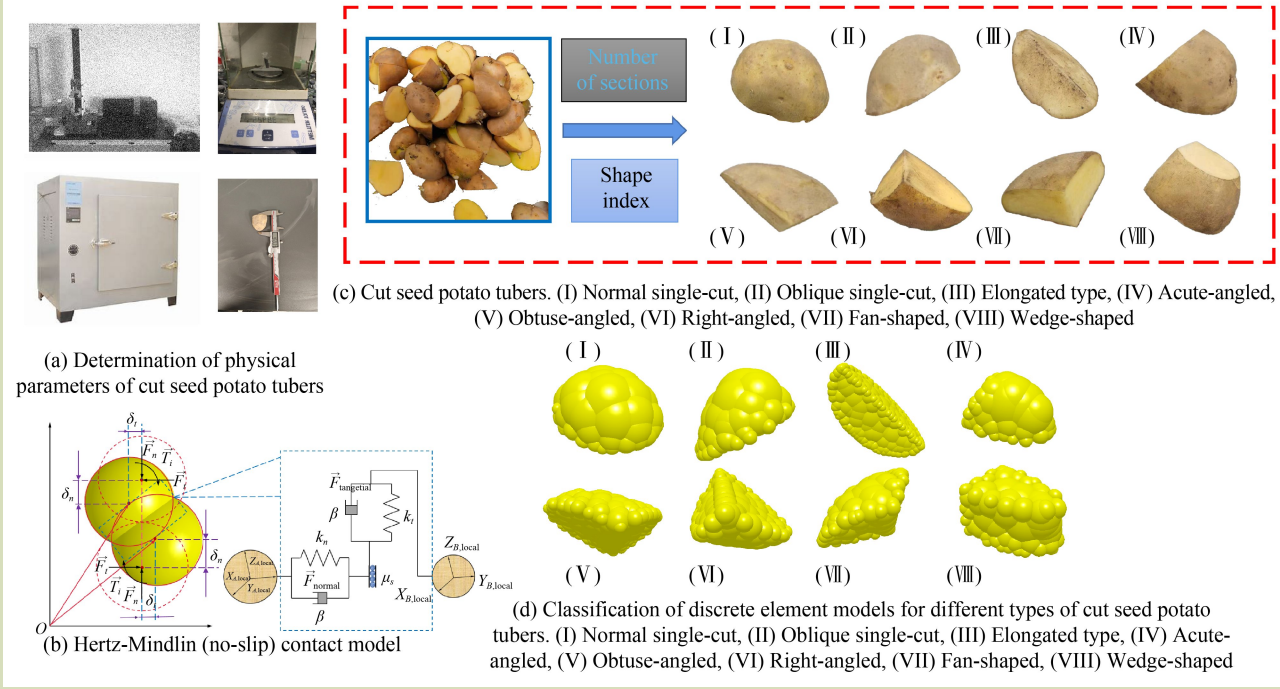
where, f_s is shape index, $a_{\max}$ is the maximum length measured along one principal orthogonal direction (mm), $b_{\max}$ is the maximum width measured along the second principal orthogonal direction (mm) and $c_{\max}$ is the maximum thickness measured along the third principal orthogonal direction (mm).

Density is a key physical property of cut seed potato tubers, defined as mass per unit volume and determined using the water-displacement method:

$$\rho = \frac{m}{V_1 - V_0} \quad (2)$$

Table 1 Measured geometric characteristics of cut seed potato tubers classified by the number of cut surfaces

Category	Single-cut-surface tubers			Double-cut-surface tubers			Triple-cut-surface tubers		
	Length (mm)	Width (mm)	Thickness (mm)	Length (mm)	Width (mm)	Thickness (mm)	Length (mm)	Width (mm)	Thickness (mm)
Maximum dimension	65.1	56.4	46.0	74.4	57.8	39.4	63.8	49.8	57.1
Minimum dimension	42.7	41.3	25.7	47.3	34.1	15.8	46.7	36.3	29.9
Mean value	58.9	48.9	32.2	55.3	44.0	27.3	56.5	40.9	37.1
Mean shape index		227			237			232	



(a) Determination of physical parameters of cut seed potato tubers

(b) Hertz-Mindlin (no-slip) contact model

(c) Cut seed potato tubers. (I) Normal single-cut, (II) Oblique single-cut, (III) Elongated type, (IV) Acute-angled, (V) Obtuse-angled, (VI) Right-angled, (VII) Fan-shaped, (VIII) Wedge-shaped

(d) Classification of discrete element models for different types of cut seed potato tubers. (I) Normal single-cut, (II) Oblique single-cut, (III) Elongated type, (IV) Acute-angled, (V) Obtuse-angled, (VI) Right-angled, (VII) Fan-shaped, (VIII) Wedge-shaped

Fig. 1 Determination of intrinsic parameters and establishment of discrete element model.

where, ρ is density of seed potatoes (kg·m^{-3}), m is mass of cut seed potato tuber (g), V_0 is volume reading of the graduated cylinder filled with water (mm^3) and V_1 is stable volume reading after immersion (mm^3).

During the test, a cut seed potato tuber was randomly selected and weighed to obtain its mass using an AL204 electronic balance (Mettler Toledo Instruments Co., Ltd.) with an accuracy of 0.1 mg (Fig. 1(a)) The sample was then fully submerged in a graduated cylinder containing a known initial water volume. After the meniscus stabilized, the final volume reading was recorded. Subsequently, the density of the tuber was calculated using Eq. 2. The procedure was repeated ten times, resulting in density values of 1190 to 1220 kg·m^{-3}, with a mean of 1200 kg·m^{-3}.

Moisture content is an important material property affecting the contact and flow properties of cut seed potato tubers. Therefore, the moisture content of the experimental materials was determined according to GB/T 3543.6-2025[32]. A DHG-9240A electric thermostatic forced-air drying oven (Shanghai Qixin Scientific Instrument Co., Ltd., Shanghai, China) and aluminum boxes were used for the measurement. Considering the large size and high moisture content of the cut seed potato tubers, the samples were prepared by cutting them into small pieces before drying. The samples were dried at 103 °C for 17 h, and the moisture content was calculated on a wet basis. Based on the measurements, the average moisture content of the experimental cut seed potato tubers was 83.83% (wet basis).

A DEM model of cut seed potato tubers was established in EDEM based on the Hertz-Mindlin (no-slip) contact model[33] (Fig. 1(b)). In practical planting operations, the cut seed potato tubers are typically dusted with a seed dressing before planting, which reduces adhesive effects during contact, prevents diseases and improves germination. The normal and tangential contact forces (F_n and F_t) for particle-particle and particle-wall interactions have the following relationships:

$$\begin{cases} F_n = \dfrac{4}{3} E^* \sqrt{R^*} \delta_n^{\frac{3}{2}} \\ F_t = -S_t \delta_t \end{cases} \tag{3}$$

where, E^* is equivalent elastic modulus (Pa), R^* is equivalent contact radius (m), δ_n is normal overlap displacement (m), δ_t is tangential overlap displacement (m) and S_t is tangential stiffness (N·m^{-1}).

Each cut seed potato tuber was modeled as an assembly of spherical particles. Contact properties for particle-particle and particle-boundary interactions were described using the governing mechanical equations. The normal and tangential damping forces, denoted by $F^d{}_n$ and $F^d{}_t$, respectively, satisfy the following relationships:

$$\begin{cases} F_n^d = -2\sqrt{\dfrac{5}{6}}\beta\sqrt{S_n m^*}\, v_n^{rel} \\ F_t^d = -2\sqrt{\dfrac{5}{6}}\beta\sqrt{S_t m^*}\, v_t^{rel} \end{cases} \tag{4}$$

where, $F^d{}_n$ is normal damping force (N), $F^d{}_t$ is tangential damping force (N), β is damping ratio, m^* is equivalent mass (g), S_n is normal stiffness (N·m^{-1}), $v^{rel}{}_n$ is normal relative velocity (m·s^{-1}) and $v^{rel}{}_t$ is tangential relative velocity (m·s^{-1}).

These parameters are given as:

$$\begin{cases} \beta = \dfrac{\ln e}{\sqrt{\ln^2 e + \pi^2}} \\ S_n = 2E^*\sqrt{R^*\delta_n} \\ S_n^* = 8G^*\sqrt{R^*\delta_n} \\ G^* = \left(2-\nu'^2\right)/G_1 + \left(2-\nu''^2\right)/G_2 \end{cases} \tag{5}$$

where, $G^*$is the equivalent shear modulus, G_1 and G_2 are the shear moduli of the two contacting bodies, and ν' and ν'' are their Poisson's ratios.

The tangential force (F_t) is additionally constrained by the Coulomb friction (f) criterion:

$$f = \mu_s F_n \tag{6}$$

where, μ_s is static friction coefficient.

Rolling friction is characterized by the resisting moment T_i at thecontact interface, given as:

$$T_i = -\mu_r F_n R_i \omega_i \tag{7}$$

where, μ_r is rolling friction coefficient, R_i is distance from centroid to contact point (m), and ω_i is angular velocity at contact point(rad·s^{-1}).

As shown in Fig. 1(c), cut seed potato tubers present substantial geometric variability, and both the external skin and cut surfaces may contact the metering components during seeding. Such shape differences are therefore incorporated into the DEM model through a hierarchical classification scheme, from which representative geometries were reconstructed (Fig. 1(d)). Table 1 gives the statistical results for the three

primary categories classified by the number of cut surfaces and Fig. 1(c,d) further illustrate representative morphological subtypes within these categories for DEM model construction.

Specifically, samples were first grouped by the number of cut surfaces and then further subdivided to improve model fidelity. Single-cut-surface tubers were classified as normal single-cut or oblique single-cut according to their deviation from a hemispherical form. Double-cut-surface tubers were identified as elongated or fan-shaped, and fan-shaped tubers were further divided into acute-, obtuse-and right-angled types based on the cut-surface angle. Triple-cut-surface tubers were categorized as fan-shaped or wedge-shaped according to the relative positions of the cut surfaces. Representative DEM clumps were generated from physical specimens for each subtype, as shown in Fig. 1(d).

2.2 Determination of physical parameters of cut seed potato tuber for DEM simulation

2.2.1 Test design for determination of coefficient of restitution

In this study, the coefficient of restitution for tuber-steel plate was determined using a drop test. Briefly, a sample was released from an initial drop height (H_a) above a steel plate and allowed to fall freely under gravity. After impact, the rebound height (H_b) was measured as the maximum height reached by the sample. The impact event was recorded using a high-speed camera at 100 frames s^{-1} (Fig. 2).

Given that cut seed potato tubers are geometrically irregular, impacts with the cut face oriented downward often produce multi-point or off-axis contacts. This can induce rotation and lateral motion, compromising the assumption of a predominantly vertical rebound. Therefore, to improve repeatability and maintain an approximately vertical rebound, the coefficient of restitution was measured by dropping samples with the uncut surface facing downward. This orientation was adopted as a standardized calibration conditions to improve measurement repeatability, rather than to fully represent all random impact orientations occurring in actual seed-metering processes. Therefore, the calibrated parameters were further validated through the angle-of-repose test and the electromagnetic vibrating feeder test, where more complex multi-attitude interactions were involved.

By definition, the coefficient of restitution is the ratio of the normal relative velocity immediately after separation to that immediately before impact and is expressed as:

$$e_1 = \frac{v_b}{v_a} = \frac{\sqrt{2gH_b}}{\sqrt{2gH_a}} = \sqrt{\frac{H_b}{H_a}} \tag{8}$$

where, e_1 is restitution coefficient between cut-seed potatoes

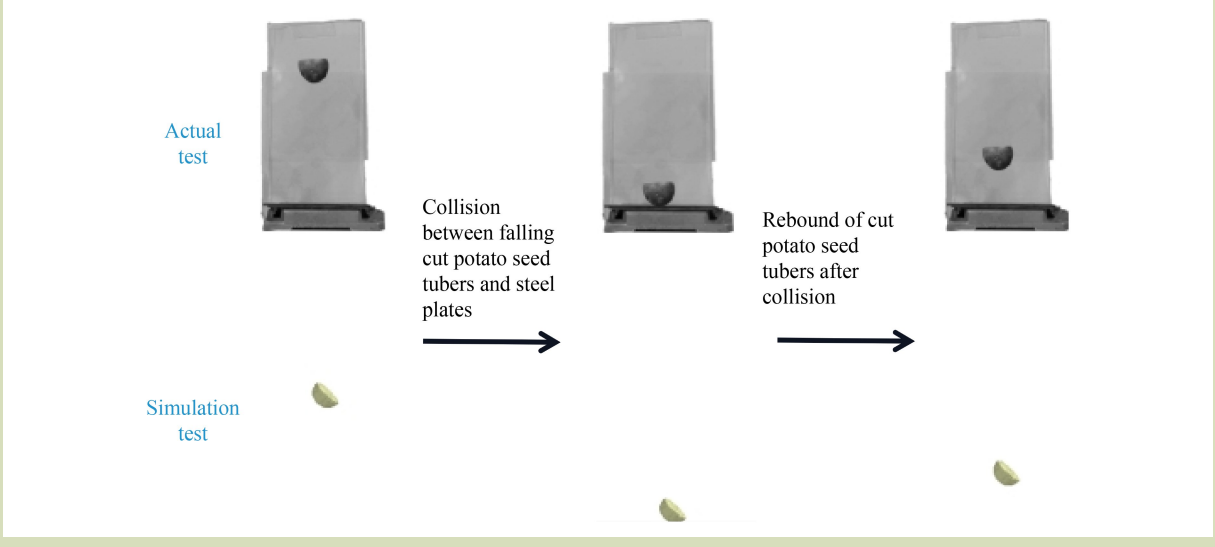


Fig. 2 Determination of coefficient of restitution between cut potato seed tubers and steel plates using drop method.

and steel plate, v_a is instantaneous velocity at impact (mm·s^{-1}), v_b is instantaneous velocity at separation (mm·s^{-1}), H_a is relative release height (mm) and H_b is maximum rebound height after collision (mm).

To improve the accuracy of the test, three release heights (300, 350 and 400 mm) were selected, and five repeated trials were conducted at each height. The measured average maximum rebound heights (H_b) were 144 ± 3.3, 175 ± 4.8 and 202 ± 6.7 mm, respectively. The corresponding coefficients of restitution for collisions between cut seed potato tuber-steel plate collisions were calculated as 0.694 ± 0.0079, 0.707 ± 0.0097 and 0.710 ± 0.012, respectively. The small variation among these values indicates that the release height has a minimal effect on the coefficient of restitution. Therefore, a release height of 350 mm was selected for DEM calibration.

A DEM model of a single-cut-surface cut seed potato tuber was selected and the model was released in free fall with an initial velocity of 0 m·s^{-1}. Both static and rolling friction coefficients were set to zero to avoid interference. Based on the experimentally determined coefficient of restitution range (0.684–0.726) at this height, parameters within this range were selected for the DEM simulation. The maximum rebound height after impact was then measured using the DEM analysis module (Fig. 3).

A fitted relationship between the coefficient of restitution and the maximum post-impact rebound height was obtained as:

$$y = 135.71429x^2 + 69.94286x + 57.78175 \quad (9)$$

The fitted model achieved an excellent goodness of fit (R^2 = 0.996), indicating a strong agreement between the regression and the simulation data. Substituting the measured rebound height with 175.18 mm in the fitted equation yielded x = 0.707. This value was then adopted as the tuber-steel plate coefficient of restitution in the DEM model.

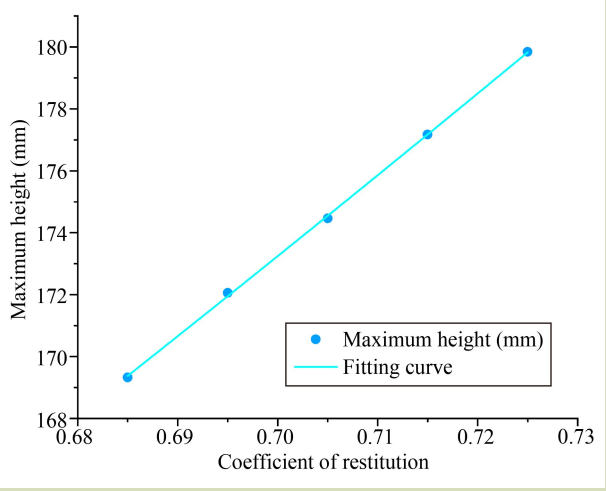


Fig. 3 Simulation test on coefficient of restitution between cut potatoes and Grade 45 steel.

To validate the calibration, additional simulations were conducted at release heights of 300, 350 and 400 mm. The corresponding maximum rebound heights were 146, 175 and 205 mm, respectively. Compared with the experimental results, the relative errors in rebound height were 0.70%, 0.05% and 1.89%. These results demonstrate that the calibrated DEM predictions are in close agreement with the physical measurements. Therefore, the coefficient of restitution for cut seed potato tuber-steel plate contact was set to 0.707.

The coefficient of restitution between cut seed potato tubers was determined by combining the pendulum test with DEM simulations. The experimentally measured post-collision rise heights were substituted into the fitted regression equations to obtain the calibrated value (Fig. 4).Two tubers (Tubers 1 and 2) were each suspended by a nylon string 500 mm in length, with the upper ends fixed to a rigid support. This configuration constrained the motion to a planar swing and enabled controlled collisions. During the test, Tuber 2 was kept at its equilibrium position (reference height of 0 mm). Tuber 1 was lifted to an initial height H_0 and then released. It swung downward and collided with Tuber 2 at the lowest point of the trajectory. After impact, both tubers continued swinging upward to reach their respective maximum heights, denoted as H_1 and H_2.

By definition, the coefficient of restitution is the ratio of the relative normal velocity immediately after separation to that immediately before impact at the contact point and is calculated as:

$$e_2 = \frac{u_2 - v_2}{v_1 - u_1} = \frac{\sqrt{2gH_2} - \sqrt{2gH_1}}{\sqrt{2gH_0}} = \frac{\sqrt{H_2} - \sqrt{H_1}}{\sqrt{H_0}} \quad (10)$$

where, e_2 is restitution coefficient between cut seed potato tubers, v_1 is instantaneous pre-impact velocity of cut seed potato tuber 1 (mm·s^{-1}), v_2 is instantaneous post-impact separation velocity of cut seed potato tuber 1 (mm·s^{-1}), u_1 is instantaneous pre-impact velocity of cut seed potato tuber

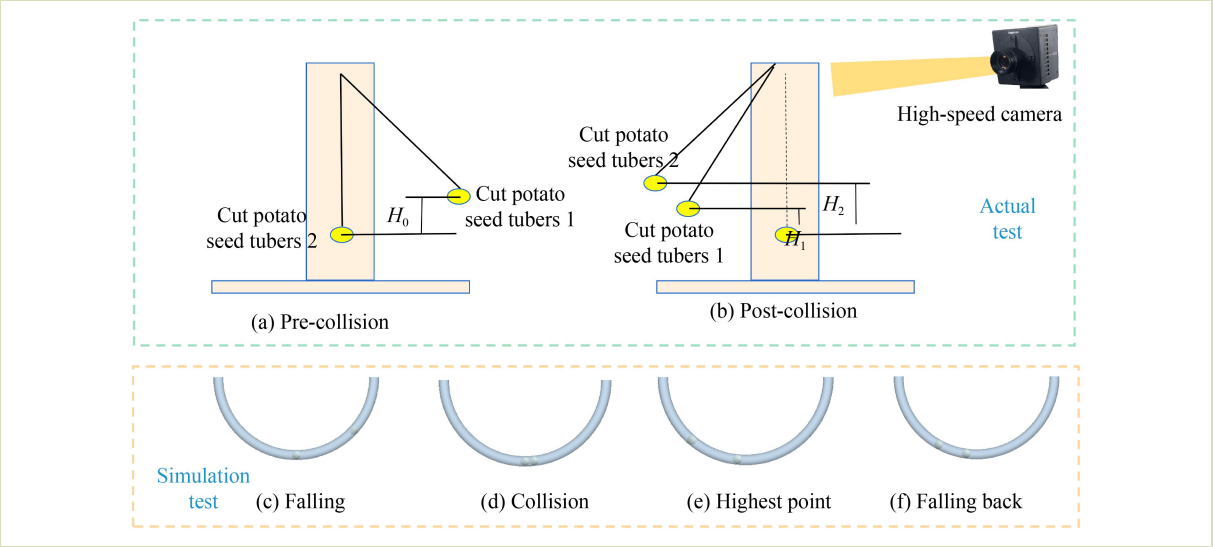


Fig. 4 Determination of coefficient of restitution between cut potato seed tubers using pendulum method.

2 (mm·s^{-1}), u_2 is instantaneous post-impact separation velocity of cut seed potato tuebr 2 (mm·s^{-1}), H_0 is initial release height of cut seed potato tuber 1 (mm), H_1 is maximum rebound height of cut seed potato tuber 1 (mm) and H_2 is maximum rebound height of cut seed potato tuber 2 (mm).

To improve measurement accuracy, three release heights (60, 80 and 100 mm) were tested, with five replicates of each. The measured maximum post-collision rises of Tuber 2 (H_2) were 50.6 ± 1.2, 68.5 ± 2.5 and 87.8 ± 0.26 mm, respectively. The corresponding maximum rises of Tuber 1 (H_1) were 1.14 ± 0.028, 1.77 ± 0.056 and 2.26 ± 0.081 mm. The calculated coefficients of restitution for tuber-tuber collisions were 0.781 ± 0.014, 0.776 ± 0.034 and 0.787 ± 0.042. The small variation among these values indicates that the release height has a negligible effect on coefficient of restitution. Therefore, 100 mm was selected for DEM calibration.

Directly reproducing the string-constrained pendulum motion in EDEM is challenging. Moreover, for a given material pair, the coefficient of restitution primarily depends on material properties rather than particle shape. Therefore, spherical surrogate particles were used to simplify the simulation. The motion was constrained by a semicircular guide (radius of 500 mm and inner diameter of 30 mm) with its centerline perpendicular to the horizontal plane. The spherical surrogate particles were used only in the pendulum-based restitution calibration to simplify the constrained collision trajectory. The final DEM validation for bulk flow and conveying properties was still performed using the non-spherical cut seed potato models established in this study.

The tubers were modeled as spheres with a diameter of 28 mm. Tuber 1 was positioned at the lowest point of the guide and Tuber 2 was placed 60 mm above that point; both were initially at rest. The coefficient of restitution and the friction coefficients between the particles and the guide were set to zero. The guide material was set as steel. At the beginning of the simulation, Tuber 2 was released with an initial velocity of 0 m·s^{-1} and collided with Tuber 1 at the bottom of the guide. The maximum post-collision rise heights of Tubers 1 and 2 (H_1 and H_2) were then obtained using the EDEM analysis module.

Simulations were conducted for a range of restitution coefficients and the corresponding maximum rise heights (H_1 and H_2) are shown in Fig. 5. Using H_1 and H_2 as response variables and e as the independent variable, second-order polynomial regressions were fitted to the simulation results. The coefficients of determination were R_1^2 = 0.990 and R_2^2 = 0.999, respectively, indicating an excellent fit. The resulting equations are:

$$\begin{cases} H_1 = 184.59 - 294.24e + 217.71e^2 \\ H_2 = 82.31 - 180.88e + 100.57e^2 \end{cases} \quad (11)$$

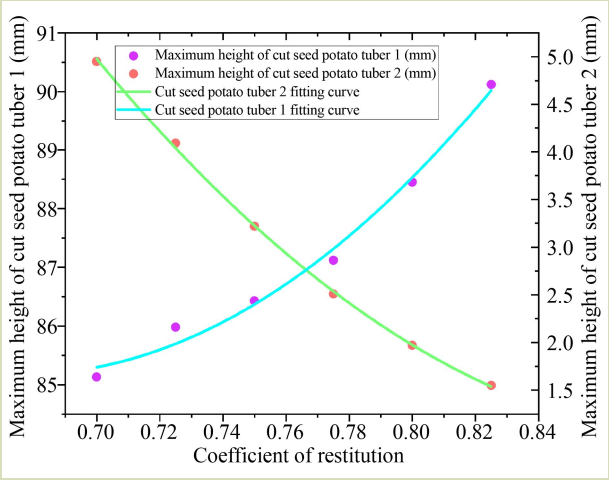


Fig. 5 Simulation test on coefficient of restitution between cut seed potato tubers.

Substituting the measured mean values (H_1 = 2.26 mm and H_2 = 87.8 mm) into the fitted equations yielded e = 0.786. This value was then assigned as the coefficient of restitution for tuber-tuber collisions in the DEM model and additional simulations were performed for validation.

Simulations were conducted at release heights of 60, 80 and 100 mm. The predicted maximum rise heights of Tuber 2 were 49.43, 67.82, and 86.45 mm, corresponding to relative errors of 2.35%, 0.93% and 1.57% with respect to the experimental measurements. The predicted maximum rise heights of Tuber 1 were 1.06, 1.71 and 2.18 mm, with relative errors of 7.01%, 3.38% and 3.54%, respectively. Overall, the calibrated DEM results are in close agreement with the experiments. Therefore, the coefficient of restitution for tuber-tuber collisions was set to 0.79.

2.2.2 Test design for determination of friction coefficient between cut seed potato tuber and steel plates

The interaction between cut seed potato tubers and the steel plate was characterized by the static and rolling friction coefficients. The static friction coefficient was measured using an inclined-plane test. For a specimen on an incline, gravity is resolved into a normal component and a tangential component along the plane. When the inclination angle is below the critical sliding angle, the specimen remains stationary. Sliding initiates when $\alpha \geqslant \alpha_0$. The static friction coefficient is then calculated as:

$$\mu_s = \frac{f_a}{N} = \frac{mg\sin\alpha_0}{mg\cos\alpha_0} = \tan\alpha_0 \tag{12}$$

where, f_a is static friction force between cut seed potato tuber material and inclined plane (N), N is normal force acting on the cut seed potato tuber (N) and α_0 is critical sliding angle (°).

In the physical test (Fig. 6, left), a Grade 45 steel plate was used as the inclined surface. The plate angle was increased slowly until the specimen began to slide. The critical angle was

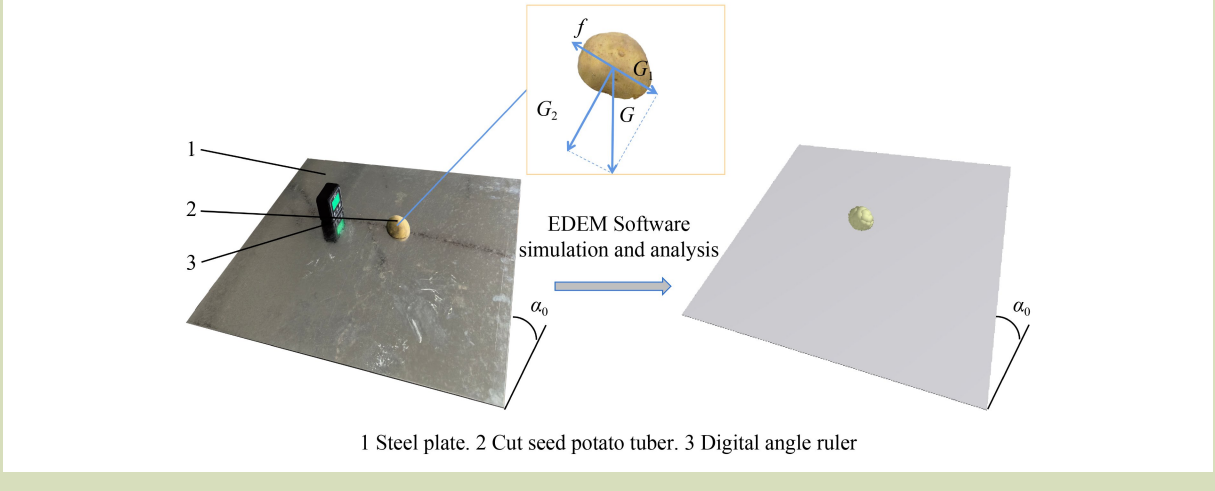


Fig. 6 Determination of the friction coefficient of cut seed potato tuber.

measured using a digital angle ruler. Ten replicate runs were conducted and averaged.

The same procedure was simulated in EDEM (Fig. 6, right). The plate material was set to Grade 45 steel, and particles consistent with the experimental specimens were generated on the plate. To isolate sliding properties, the rolling friction coefficient between the particles and the plate was set to 0, and the coefficient of restitution was set to 0.707. The inclination angle was increased until sliding occurred, and α_0 was recorded. Five simulation replicate runs were performed and the mean value used.

Rolling resistance was quantified using the rolling friction coefficient. The inclined-plane rolling method was adopted. The plate angle was increased gradually until the specimen began to roll as a whole, and the corresponding critical rolling angle was measured with the digital angle ruler. The test was repeated ten times. The rolling friction coefficient was calculated as:

$$\mu_r = \frac{f'}{N'} = \frac{mg\sin\alpha_1}{mg\cos\alpha_1} = \tan\alpha_1 \tag{13}$$

where, f' is static friction force between cut seed potato tuber and inclined plane (N), N' is normal force acting on the cut seed potato tuber (N) and α_1 is steady rolling angle (°).

The rolling test was also implemented in EDEM using the same setup and procedure. Five replicate runs were conducted and the mean value used.

Finally, the static friction coefficient between the cut seed potato tubers and the steel plate was measured as 0.445, while the rolling friction coefficient was 0.269.

2.3 Test design using Plackett-Burman, steepest ascent and Box-Behnken methods

Given that the pronounced shape variability of cut seed potato tubers, the inter-tuber friction coefficients are difficult to measure directly. Therefore, an indirect approach was adopted to determine the inter-tuber friction characteristics. The angle of repose is a key parameter describing the flowability and frictional properties of granular materials, and it is related to the static and rolling friction coefficients. In this study, the experimentally measured angle of repose was used as the target value. A DEM model was established using the previously measured contact parameters between cut seed potato tubers and the steel plate, including the static friction coefficient, rolling friction coefficient and coefficient of restitution. Under the same test conditions, the inter-tuber static and rolling friction coefficients were then estimated through DEM calibration.

The angle of repose was measured using the cylindrical lifting method. A bottomless cylinder (inner diameter of 300 mm and height of 550 mm) was placed on a horizontally positioned Grade 45 steel plate (1 m × 1 m). A SH3-103 high-speed camera (Shenzhen SinceVision Technology Co., Ltd., Shenzhen, Guangdong, China) was used to record the piling process at 125 frames s^{-1}. Cut seed potato tubers were loaded into the cylinder, which was then lifted vertically at a speed of 50 mm·s^{-1} until a stable pile was formed on the plate. The test was repeated ten times. The angle of repose was then measured (Fig. 7), and the final mean value was 26.7°.

Details of the tuber-plate used in this study are given in Table 2. As Poisson's ratio and shear modulus had a negligible influence on the simulated angle of repose in this study, Poisson's ratio and shear modulus were set to 0.35 and 1.34 MPa, respectively, based on values reported in the literature[12].

The bottomless cylinder and steel plate were imported into EDEM with dimensions matching the experimental setup. Particles were generated from the top of the cylinder at 200 particles·s^{-1} for 5 s. After the system reached a stable state, the cylinder was lifted upward at 50 mm·s^{-1} for 5 s, allowing particles to discharge and form a stable pile (Fig. 7). The angle of repose was obtained using the built-in angle measurement tool in EDEM. Friction coefficients were then calibrated by matching the simulated angle of repose to the experimental value.

Based on preliminary research, pre-simulation tests and a review of the literature[12], the level ranges of various factors for cut seed potato tubers were determined (Table 3).

The Design-Expert software, version 13.0 (Stat-Ease, Inc., Minneapolis, MN, USA), was used to perform a Plackett-Burman screening design, followed by a steepest-ascent experiment, with the simulated angle of repose of the cut seed potato tubers as the response variable. This procedure was used

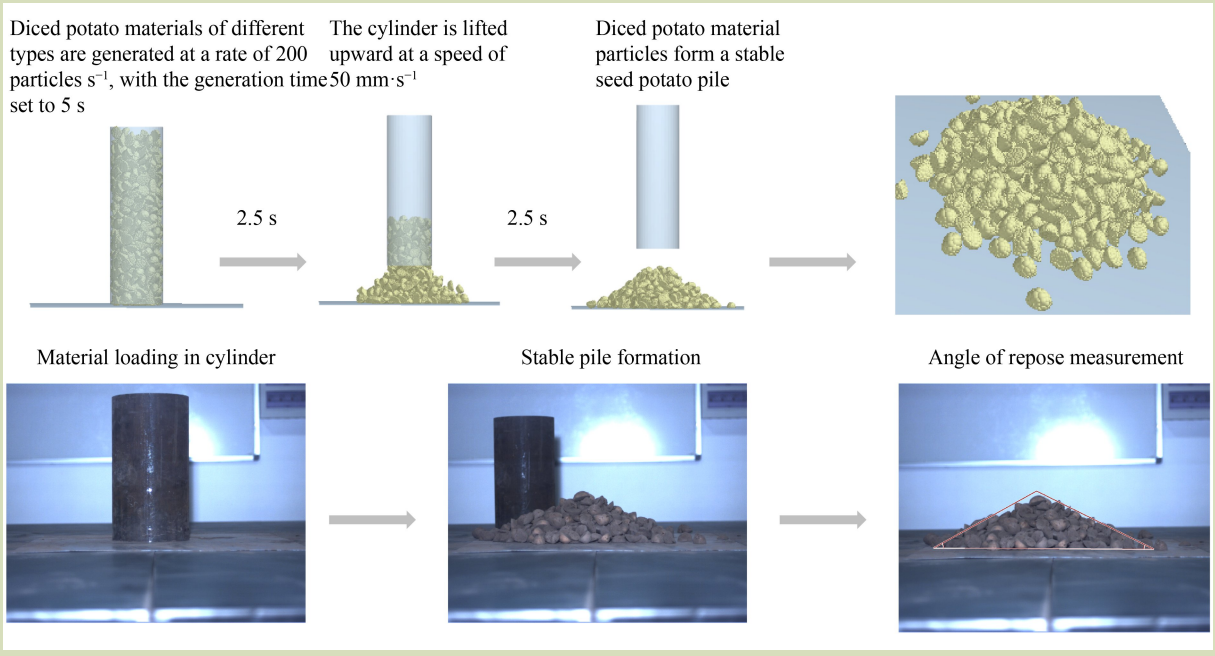


Fig. 7 Practical tests and simulation tests of the cylinder lifting method.

Table 2 Physical parameters of cut seed potato tubers and steel

Serial number	Parameter	Value
1	Poisson's ratio of cut seed potato tubers	0.35
2	Density of cut seed potato tubers	1201.87 kg·m^{-3}
3	Shear modulus of cut seed potato tubers	1.34 MPa
4	Poisson's ratio of steel	0.3
5	Density of steel	7.8×10^{3} kg·m^{-3}
6	Shear modulus of steel	7.9×10^{4} MPa
7	Restitution coefficient between cut seed potato tubers	0.79
8	Restitution coefficient between cut seed potato tubers and steel	0.71
9	Static friction coefficient between cut seed potato tubers and steel	0.445
10	Rolling friction coefficient between cut seed potato tubers and steel	0.269

to identify the significant factors influencing the angle of repose and to guide subsequent optimization.

For the DEM simulations, model parameters were initialized using measured values. Based on preliminary tests, published studies and the screening results, a Box-Behnken design was established with the factor levels given in Table 4. The selected variables were consistent with those identified as significant in the screening stage. Analysis of variance (ANOVA) was conducted in Design-Expert to evaluate the significance of model terms and the adequacy of the fitted response surface.

2.4 Design of discrete element parameter simulation and verification test based on electromagnetic vibratory seed feeding device

To validate the calibrated DEM parameters for cut seed potato tubers, EDEM simulations were conducted and the results were

Table 3 Parameter level table of Plackett-Burman test

Serial number	Test factor	Level	
		−1	+1
X_1	Coefficient of restitution between cut seed potato tubers and steel	0.6	0.8
X_2	Static friction coefficient between cut seed potato tubers and stee	0.3	0.6
X_3	Rolling friction coefficient between cut seed potato tubers and steel	0.25	0.29
X_4	Coefficient of restitution between cut seed potato tubers	0.7	0.9
X_5	Static friction coefficient between cut seed potato tubers	0.3	0.5
X_6	Rolling friction coefficient between cut seed potato tubers	0.01	0.03

Table 4 Optimization test design and results

Level	Static friction coefficient between cut seed potato tubers and steel plate X_2	Static friction coefficient between cut seed potato tubers X_5	Rolling friction coefficient between cut seed potato tubers X_6
1	0.477	0.470	0.025
0	0.445	0.460	0.023
−1	0.413	0.450	0.021

experimentally verified using an electromagnetic vibration-based potato seed-metering device.

2.4.1 Establishment of EDEM discrete element simulation model for electromagnetic vibratory seed feeding device

The EDEM software enables direct visualization of cut seed potato tuber motion and conveying properties, and the built-in analysis module provides quantitative outputs such as velocity and kinetic energy. In the DEM model, the system consisted of cut seed-tuber particles and the feeding device. The component directly interacting with the particles was the vibrating hopper; therefore, the vibrator (exciter) itself was not modeled explicitly. Instead, the measured excitation was imposed as prescribed motion on the hopper in EDEM, which reproduces the effect of the exciter while reducing model complexity.

The hopper motion driven by the exciter can be regarded as a superposition of vertical vibration and circumferential (torsional) oscillation. Accordingly, sinusoidal motion functions were applied in the vertical and circumferential directions, with vertical amplitude z_0 and angular amplitude ϕ_0, respectively:

$$\begin{cases} Z(t) = z_0 \sin(2\pi f_{Hz} \cdot t) \\ \phi(t) = \phi_0 \sin(2\pi f_{Hz} \cdot t) \end{cases} \tag{14}$$

where, z_0 is vertical amplitude (mm), φ_0 is angular amplitude (rad·s^{-1}) and f_{Hz} is vibration frequency (Hz).

In this study, the operating frequency range of the vibrating feeding device was 40–100 Hz, and the excitation frequency was set to 50 Hz to reduce the risk of resonance and ensure sub-resonant operation. Given that the main vibration spring constrains the hopper, z_0 and ϕ_0 are not independent and satisfy the following relationship:

$$\phi_0 = \frac{z_0}{r_A \tan\phi_A} \cdot \frac{180}{\pi} \tag{15}$$

where, r_A is spring installation radius (mm) and ϕ_A is spring installation angle (°).

In DEM simulations, particle forces are assumed constant within each time step. An excessively large time step reduces accuracy whereas an overly small time step increases computational cost. The simulation time step was set to 20% of the Rayleigh time step and the integration time step T_R was determined as:

$$T_R = \pi R\left(\frac{\rho}{G}\right)^{\frac{1}{2}} (0.1631\mu + 0.8766) \tag{16}$$

where, T_R is time step (s), R is particle radius (m), G is shear modulus of the particle material (Pa) and μ is Poisson's ratio of the particle material.

The vibration amplitude is approximately proportional to the operating voltage. The vertical amplitude z_0 was measured at different voltages, and the corresponding ϕ_0 values were calculated using the above relationship. The resulting voltage-amplitude mapping is given in Table 5.

2.4.2 Establishment of the electromagnetic vibratory seed feeding device

The electromagnetic vibration hopper and exciter of the vibration-based seed-feeding device were fabricated and assembled, and the prototype is shown in Fig. 8. The hopper was made with Grade 45 steel. The vibration amplitude was regulated using an SDVC20-S intelligent digital vibration controller, with an input voltage of 150–260 V, an output voltage of 30–250 V, an output current of 0–5 A and a voltage adjustment resolution of 1 V. The hopper height was 240 mm, and the maximum diameter was 500 mm. The excitation frequency was set to 50 Hz to match the DEM simulations. The pitch and bottom inclination angle were set to the optimal combination obtained from the response surface analysis to enable direct comparison with the simulation results. Cut seed

Table 5 Corresponding relationship between vertical amplitude, angular amplitude and vibrator voltage

Serial number	Working voltage (V)	Vertical amplitude (mm)	Angular amplitude (°)
1	110	1.89	0.516
2	120	2.27	0.621
3	130	2.65	0.724
4	140	3.01	0.822
5	150	3.35	0.915
6	160	3.71	1.014
7	170	4.09	1.12



Fig. 8 Prototype of the electromagnetic vibration seed-feeding device.

potato tubers from the same batch of cv. Dutch No. 15 used for parameter calibration were used. The test duration was recorded using a Tianfu PC2810 stopwatch (resolution of 0.01 s).

2.4.3 Design of simulation and verification test

In the DEM simulations, the proportions of the single-, double- and triple-cut-surface tuber models were set to be consistent with those used in the physical sampling. For all simulations, the integration time step was set to 20% of the Rayleigh time step, the data saving interval was 0.01 s, and the total simulation time was 60 s. The mesh opening was set to three times the minimum radius of the constituent spherical elements.

Both DEM and physical tests were performed using the same electromagnetic vibrating hopper. In the first test, 60 randomly selected cut seed potato tubers were loaded and the total discharge time was recorded at operating voltages from 110 to 170 V in 10 V increments. Each set of conditions was repeated five times and mean values were compared with the simulation results. In the second test, 120 tubers were loaded and the mass flow rate was measured over the same voltage range. Five replicate runs were conducted for each voltage and the averaged mass flow rates were compared with DEM predictions.

3 Results

3.1 Results of Plackett-Burman, steepest ascent, and Box-Behnken tests

The experimental design and corresponding results are given in Table 6, comprising 12 runs.

The ANOVA results are given in Table 7. The model was statistically significant ($p < 0.01$), indicating that the fitted response adequately explains the observed variation. The coefficient of determination was $R^2 = 0.963$, and the adjusted coefficient of determination was $R_{adj}^2 = 0.919$. The coefficient of variation (CV) was 1.12%, indicating good experimental precision.

Of the investigated factors, the tuber-steel plate static friction coefficient (X_2) had a significant effect on the simulated angle of repose. In addition, the inter-tuber static friction coefficient (X_5) and inter-tuber rolling friction coefficient (X_6) were highly significant. The influence of the remaining parameters were comparatively minor. Based on the steepest-ascent results and using the measured angle of repose as the target response, the search ranges (gradient intervals) for the significant factors were subsequently determined.

The Box-Behnken design and corresponding responses are given in Table 8.

Table 6 Plackett-Burman experimental scheme and results

Test number	X_1	X_2	X_3	X_4	X_5	X_6	Angle of repose (°)
1	1	1	−1	1	1	1	30.17
2	−1	1	1	−1	1	1	30.16
3	1	−1	1	1	−1	1	28.14
4	−1	1	−1	1	1	−1	28.01
5	−1	−1	1	−1	1	1	28.82
6	−1	−1	−1	1	−1	1	28.12
7	1	−1	−1	−1	1	−1	27.68
8	1	1	−1	−1	−1	1	28.54
9	1	1	1	−1	−1	−1	27.13
10	−1	1	1	1	−1	−1	27.09
11	1	−1	1	1	1	−1	27.64
12	−1	−1	−1	−1	−1	−1	26.74

Table 7 Significance analysis of Plackett-Burman test parameters

Source of variance	Sum of square	Degrees of freedom	Mean square	*p*-value
Model	12.87	6	2.14	0.0020**
X_1	0.0108	1	0.0108	0.7545
X_2	1.31	1	1.31	0.0150*
X_3	0.0065	1	0.0065	0.8074
X_4	0.0008	1	0.0008	0.9304
X_5	3.76	1	3.76	0.0016**
X_6	7.78	1	7.78	0.0003**
Residual	0.4946	5	0.0989	

Note: * $p < 0.05$; ** $p < 0.01$.

Table 8 Optimization test design and results

Test number	X_2	X_5	X_6	Angle of repose (°)
1	0	0	0	28.28
2	0	0	0	28.43
3	0	1	1	29.63
4	–1	1	0	28.45
5	–1	–1	0	25.32
6	1	1	0	28.76
7	1	0	–1	27.78
8	0	0	0	28.26
9	–1	0	1	28.21
10	0	1	–1	27.72
11	0	0	0	28.21
12	0	–1	1	25.83
13	1	–1	0	25.69
14	0	0	0	28.25
15	0	–1	–1	26.18
16	1	0	1	28.44
17	–1	0	–1	27.51

ANOVA of the DEM simulation results was performed in Design-Expert and the results are given in Table 9. The fitted model was highly significant ($p < 0.0001$), whereas the lack-of-fit was not significant ($p = 0.180$, which was greater than 0.05), indicating an adequate model fit. The goodness-of-fit statistics were $R^2 = 0.992$, $R_{adj}^2 = 0.982$ and CV = 0.34%, demonstrating high precision and reliability of the regression model. The relationship between the simulated angle of repose and the coded factors is described as:

$$\theta = 28.29 + 0.1475X_2 + 1.44X_5 + 0.3650X_6 - 0.015X_2X_5 - 0.01X_2X_6 + 0.565X_4X_6 - 0.2930X_2^2 - 0.9380X_3^2 - 0.008X_6^2 \quad (17)$$

For parameter optimization, the experimentally measured angle of repose (26.7°) was used as the target response. The

Table 9 Analysis of variance for the regression model

Source of variance	Sum of square	Degrees of freedom	Mean square	*p*-value
p-value	23.20	9	2.6	< 0.0001**
X_2	0.141	1	0.141	0.0183*
X_5	16.65	1	16.65	< 0.0001**
X_6	1.07	1	1.07	0.0001**
X_2X_5	0.0009	1	0.0009	0.8321
X_2X_6	0.0004	1	0.0004	0.8875
X_5X_6	1.28	1	1.28	< 0.0001**
X_2^2	0.3615	1	0.3615	0.0031**
X_5^2	3.7	1	3.7	< 0.0001**
X_6^2	0.0003	1	0.0003	0.9075
Residual	0.13	7	0.0186	

Note: * $p < 0.05$; ** $p < 0.01$; $R^2 = 0.9945$; $R_{adj}^2 = 0.9874$; CV% = 0.49%; Adeq precision = 40.7786.

tuber-plate static friction coefficient was fixed at the measured value of 0.445. Using the numerical optimization module in Design-Expert, the optimal parameter set was obtained as: X_2 = 0.445 (static friction coefficient between cut seed potato tubers and the steel plate), X_5 = 0.453 (inter-tuber static friction coefficient) and X_6 = 0.0240 (inter-tuber rolling friction coefficient).

To validate the optimal parameters obtained from the Box-Behnken design, DEM simulations of the cylindrical lifting method were performed using the calibrated contact parameters for cut seed potato tubers. Each simulation was repeated three times, and the mean angle of repose was 26.4°. This value differed from the experimental measurement by 1.27%, indicating good agreement.

3.2 Simulation and verification test of electromagnetic vibration seeding device

The DEM predictions agreed well with the physical measurements in terms of both discharge time and mass flow rate. As shown in Fig. 9, the relative errors were 4.84% and 4.07%, respectively. The good agreement between the DEM predictions and experimental results for discharge time and mass flow rate indicates that the calibrated parameter set can reliably describe the conveying properties of cut seed potato tubers in the vibrating hopper. This provides a useful basis for the structural design and parameter optimization of seed potato planting equipment, such as hopper geometry, vibration intensity, and operating voltage. In practical applications, the calibrated model may help reduce feeding blockage, improve feeding uniformity and enhance the stability of seed-metering performance.

A qualitative comparison of the feeding process is shown in Fig. 10. In both the experiments and simulations, cut seed potato tubers dispersed from the hopper bottom under vibration and gradually entered the spiral track, consistent with the observed conveying properties. Frame-by-frame analysis of the experimental videos further revealed distinct motion modes. Under the critical jumping conditions (cut surface downward), the motion sequence typically involved partial separation, complete detachment from the surface then re-contact, with one side landing on the track first. Under the critical sliding conditions, no noticeable vertical separation occurred; instead, the tubers advanced via continuous creeping along the spiral track. When the cut face was oriented downward, jumping was more pronounced and the contacting region tended to detach directly from the track. In both jumping and sliding regimes, a backward-tilting tendency was observed immediately beforehand, indicating an imminent transition.

Overall, the developed DEM representation and the calibrated contact parameters provide a reliable basis for simulating the handling and conveying of cut seed potato tubers, and may

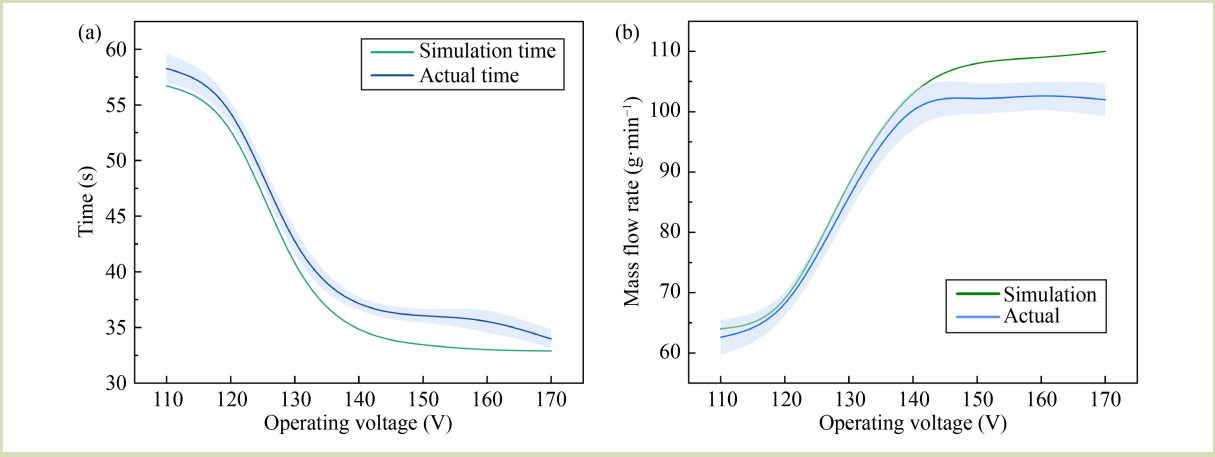


Fig. 9 Comparative curve of physical test and simulation test processes. (a) Working voltage-sorting time curve; (b) working voltage-mass flow rate curve.

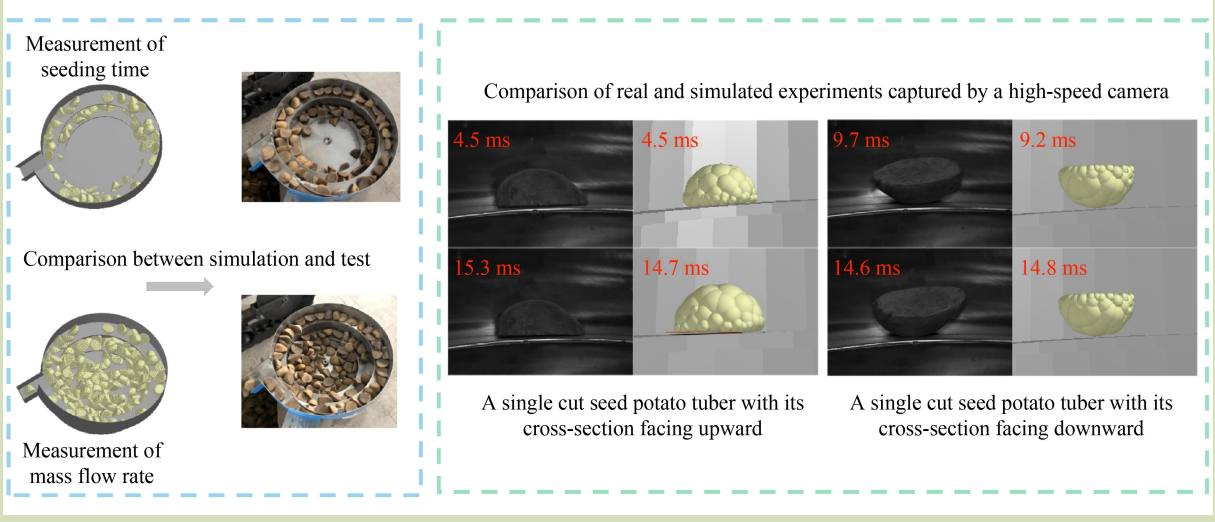


Fig. 10 Simulation test and actual test.

serve as reference data for DEM-based analyses in mechanized potato planting, harvesting and related operations.

The good agreement between the DEM predictions and experimental results for discharge time and mass flow rate indicates that the calibrated parameter set can reliably describe the conveying properties of cut seed potato tubers in the vibrating hopper. This provides a useful basis for the structural design and parameter optimization of seed potato planting equipment, such as hopper geometry, vibration intensity and operating voltage. In practical applications, the calibrated model may help reduce feeding blockage, improve feeding uniformity and enhance the stability of seed-metering performance.

4 Discussion

Accuracy is a central concern in DEM-based analyses. Reliable simulation of irregular agricultural materials, such as cut seed

potato tubers, requires both realistic geometric representation and rigorous calibration of intrinsic and contact parameters[24]. Unlike potato mini-tubers[11,12], which are often close to ellipsoids or quasi-spheres, cut seed potato tubers exhibit highly irregular shapes and multiple configurations. In this work, cut tubers were classified according to the number and arrangement of cut surfaces, and representative DEM geometries were constructed from measured dimensional data.

For irregularly shaped materials, the inter-particle coefficient of restitution is often omitted because of experimental challenges, or it is obtained through indirect calibration[15,19,27,29]. However, for cut seed potato tubers, the inter-tuber coefficient of restitution is a key parameter governing collision dynamics. Given that the pendulum test is difficult to implement directly in EDEM, a semicircular guide method was adopted to estimate the inter-tuber restitution coefficient in a manner compatible with DEM modeling.

For parameter optimization, integrated approaches combining Plackett-Burman design, the steepest ascent method and response surface methodology[27–29], as well as genetic algorithms [30], have been widely adopted and proven effective. This study used a similar approach, achieving an angle of repose error of 1.27%. With recent advances in machine learning, alternative approaches have emerged. For example, Zhao et al.[26] proposed an FNN-based regression model for angle of repose, while Ding et al.[24] developed a hybrid modeling approach integrating RSM and machine learning techniques, both yielding promising results. Future research may explore integrating such methods to further improve calibration accuracy.

Beyond the conventional angle-of-repose validation used in many studies[15,25], the calibrated parameters were additionally evaluated in an electromagnetic vibrating hopper. The relative errors in discharge time and mass flow rate were both below 5%, providing independent evidence that the calibrated parameters are reliable for simulating the conveying properties of cut seed potato tubers.

The calibrated DEM parameters obtained in this study are based on cv. Dutch No. 15 under the tested material conditions. Given that tuber size distribution, cut-surface morphology, skin texture and moisture content may differ among potato cultivars, the absolute parameter values may not be directly transferable to all cultivars. In the this study, the tested cut seed potato tubers had an average moisture content of 83.83% (wet basis), and the calibrated DEM parameters are therefore most applicable to materials under similar moisture and surface conditions. However, the proposed hierarchical modeling strategy and the calibration procedure combining physical experiments with DEM optimization are expected to be applicable to other cut seed potato cultivars. For materials with substantially different physical characteristics, the contact parameters should be recalibrated before engineering application.

5 Conclusions

In this study, the intrinsic properties of cv. Dutch No. 15 cut seed potato tubers, including geometric dimensions, density, and moisture content, were measured. Tubers were then classified according to the number of cut surfaces and the shape index, and representative DEM geometries were established accordingly. Based on physical experiments and DEM simulations, the parameter ranges for tuber-steel plate contact were determined (coefficient of restitution, static friction coefficient and rolling friction coefficient), together with the inter-tuber coefficient of restitution.

For parameters that are difficult to measure directly, a sequential calibration strategy combining Plackett-Burman screening, steepest ascent and a Box-Behnken response surface design was used. The calibrated inter-tuber static friction coefficient and rolling friction coefficient were 0.453 and 0.024, respectively. Validation using the cylindrical lifting method yielded an angle-of-repose relative error of 1.27%. Additional tests with an electromagnetic vibrating feeder further confirmed the calibration, with relative errors below 5% in mass flow rate and consistent dynamic motion properties between experiments and simulations. Overall, the proposed modeling and calibration workflow provides reliable DEM input parameters for cut seed potato tuber materials and supports the design and performance analysis of mechanized cut seed potato tuber planting equipment.

Acknowledgements

This research was funded by the Natural Science Foundation of Chongqing Municipality, China (cstc2021jcyj-msxmX1178), the

National Natural Science Foundation of China Youth Science Fund Project (No. 52205295), the Fundamental Research Funds for the Central Universities (SWU-KF25032), and the Fundamental Research Funds for the Central Universities (SWU-KF25009). In addition, we thank Professor Lihong Wang and Associate Professor Hui Li for their valuable contributions to this paper. The authors used ChatGPT (GPT-5.4 Thinking, OpenAI) for language polishing. All scientific content, data analysis, interpretation of results and final decisions were completed and verified by the authors.

Compliance with ethics guidelines

Niu Qi, Rongxiang Diao, Rui Ran, Hongnan Hu, Zhongcai Wei, Mingsheng Li, Chengsong Li, and Pei Wang declare that they have no conflicts of interest or financial conflicts to disclose. This article does not contain any studies with human or animal subjects performed by any of the authors.

REFERENCES

1. Singh C, Randhawa G S, Farooque A A, Gill Y S, Kumar KM L, Singh M, Al-Mughrabi K. Evaluation of deep learning models for RGB image-based detection of potato virus y strain symptoms (O, NO, and NTN) in potato plants. *Smart Agricultural Technology*, 2025, **10**: 100755
2. Zhou B D, Li Y X, Zhang C, Cao L W, Li C S, Xie S Y, Niu Q. Potato planter and planting technology: a review of recent developments. *Agriculture*, 2022, **12**(10): 1600
3. Food and Agriculture Organization of the United Nations (FAO). World Food and Agriculture – Statistical Yearbook 2023. Rome: *FAO*, 2023. Available at FAO website on January 19, 2024
4. Chen M D, Liu X T, Hu P X, Zhai X T, Han Z L, Shi Y L, Zhu W J, Wang D W, He X N, Shang S Q. Study on rotor vibration potato-soil separation device for potato harvester using DEM-MBD coupling simulation. *Computers and Electronics in Agriculture*, 2024, **218**: 108638
5. Chen E H, Shi L R, Sun B G. Research status and development trend of potato planters and seed platters. *Forestry Machinery & Woodworking Equipment*, 2021, **49**(7): 4–8 (in Chinese)
6. Azimi-Nejadian H, Karparvarfard S H, Naderi-Boldaji M. Weed seed burial as affected by mouldboard design parameters, ploughing depth and speed: DEM simulations and experimental validation. *Biosystems Engineering*, 2022, **216**: 79–92
7. Guzman L, Chen Y, Landry H. Coupled CFD-DEM simulation of seed flow in horizontal-vertical tube transition. *Processes*, 2023, **11**(3): 909
8. Moncada M, Betancourt F, Rodríguez C G, Toledo P. Effect of particle shape on parameter calibration for a discrete element model for mining applications. *Minerals*, 2023, **13**(1): 40
9. Sharaby N N, Doroshenko A A, Butovchenko A V. Simulation of sesame seeds outflow in oscillating seed metering device using DEM. *Engineering Technologies and Systems*, 2020, **30**(2): 219–231
10. Zhang F B, Luo Z T, Li W X, Zheng E L, Pan D C, Qian J, Yao H P, Wang X C. Structural design and optimization of crushing and strip-laying device based on discrete element method with wet-adhesive flexible straw model. *Computers and Electronics in Agriculture*, 2025, **237**: 110537
11. Liu W Z, He J, Li H W, Li X Q, Zheng K, Wei Z C. Calibration of simulation parameters for potato minituber based on EDEM. *Transactions of the Chinese Society for Agricultural Machinery*, 2018, **49**(5): 125–135, 142 (in Chinese)
12. Shi L R, Sun W, Zhao W Y, Yang X P, Feng B. Parameter determination and validation of discrete element model of seed potato mechanical seeding. *Transactions of the Chinese Society of Agricultural Engineering*, 2018, **34**(6): 35–42 (in Chinese)
13. Chen K, Yin X, Ma W P, Jin C Q, Liao Y Y. Contact parameter calibration for discrete element potato minituber seed simulation. *Agriculture*, 2024, **14**(12): 2298
14. Xu J, Wang X M, Zhang Z B, Wu W B. Discrete element modeling and simulation of soybean seed using multi-spheres and super-ellipsoids. *IEEE Access*, 2020, **8**: 222672–222683
15. Wang S, Yu Z H, Aorigele, Zhang W J. Study on the modeling method of sunflower seed particles based on the discrete element method. *Computers and Electronics in Agriculture*, 2022, **198**: 107012
16. Hoshishima C, Ohsaki S, Nakamura H, Watano S. Parameter calibration of discrete element method modelling for cohesive and non-spherical particles of powder. *Powder Technology*, 2021, **386**: 199–208
17. Wang Y B, Li H W, Hu H N, He J, Wang Q J, Lu C Y, Liu P, Yang Q L, He D, Jiang S, Huang S H. A noncontact self-suction wheat shooting device for sustainable agriculture: a preliminary research. *Computers and Electronics in Agriculture*, 2022, **197**: 106927
18. Liu G Y, Xu W J. A GPU-based DEM framework for simulation of polyhedral particulate system. *Granular Matter*, 2023, **25**(2): 27

19. He Y, Ji X X, Dun G Q, Liu X Y, Mu A K, Ma C Y. Discrete element simulation calibration of contact parameters for millet seeds. *INMATEH-Agricultural Engineering*, 2025, **76**(2): 686–696
20. Xu T Y, Fu H, Liu M, Feng W Z, Zhang R X, Wang Y, Wang J L. Ellipsoidal seed modeling and simulation parameter selection based on the discrete element method. *Materials Today Communications*, 2023, **37**: 106923
21. Dun G Q, Zhang C X, Ji X X, Meng Q J, Sheng Q B, Wang L. Simulation parameter calibration and test of pakchoi seeds based on discrete element method. *INMATEH-Agricultural Engineering*, 2024, **73**(2): 391–405
22. Yu Q X, Liu Y, Chen X B, Sun K, Lai Q H. Calibration and experiment of simulation parameters for *Panax notoginseng* seeds based on DEM. *Transactions of the Chinese Society for Agricultural Machinery*, 2020, **51**(2): 123–132 (in Chinese)
23. Wang L B, Yang H Y, Wang Z N, Wang Q J, Lu C Y, Wang C, He J. Calibration of DEM polyhedron model for wheat seed based on angle of repose test and semi-resolved CFD-DEM coupling simulation. *Agriculture*, 2025, **15**(5): 506
24. Ding X T, Wang B B, He Z, Shi Y G, Li K, Cui Y J, Yang Q C. Fast and precise DEM parameter calibration for *Cucurbita ficifolia* seeds. *Biosystems Engineering*, 2023, **236**: 258–276
25. Zhu X F, Xu Y, Han C J, Yang B N, Luo Y, Qiu S L, Huang X N, Mao H P. Parameter calibration and experimental verification of the discrete element model of the edible sunflower seed. *Agriculture*, 2025, **15**(3): 292
26. Zhao X, Bai H B, Liu F, Dong W X. DEM modelling methods and trait analysis of sunflower seed. *Biosystems Engineering*, 2025, **250**: 39–48
27. Chen X Y, Wang X Z, Bai J, Fang W Q, Hong T Y, Zang N, Wang G L. Virtual parameter calibration of pod pepper seeds based on discrete element simulation. *Heliyon*, 2024, **10**(11): e31686
28. Gao X J, Xie G F, Li J, Shi G S, Lai Q H, Huang Y X. Design and validation of a centrifugal variable-diameter pneumatic high-speed precision seed-metering device for maize. *Biosystems Engineering*, 2023, **227**: 161–181
29. Zhong J Q, Tao L M, Li S P, Zhang B, Wang J Y, He Y L. Determination and interpretation of parameters of double-bud sugarcane model based on discrete element. *Computers and Electronics in Agriculture*, 2022, **203**: 107428
30. Do H Q, Aragón A M, Schott D L. A calibration framework for discrete element model parameters using genetic algorithms. *Advanced Powder Technology*, 2018, **29**(6): 1393–1403
31. Ministry of Agriculture and Rural Affairs of the People's Republic of China. NY/T 3483-2019 Technical Specification for Mechanized Production of Potato. Beijing: *China Agricultural Press*, 2019 (in Chinese)
32. State Administration for Market Regulation, Standardization Administration of China. GB/T 3543.6-2025 Rules for Agricultural Seed Testing—Part 6: Sowing Quality—Determination of Moisture Content. Beijing: *Standards Press of China*, 2025 (in Chinese)
33. Walton O R, Braun R L. Stress calculations for assemblies of inelastic speres in uniform shear. *Acta Mechanica*, 1986, **63**(1–4): 73–86